Preliminary Geothermal Conceptual Model of the Salve Faccha-Oyacachi Prospect, Chacana Caldera, Ecuador

Danilo Asimbaya-Amaguaña[1,2], Kotaro Yonezu[1], Akane Ito[1], Danilo Ibarra[1,2], Saefudin Juhri[1], Akira Imai[1]

[1] Department of Earth Resources Engineering, Kyushu University – Japan

[2] Ecuadorian Geothermal Association

asimbaya.danilo.050@s.kyushu-u.ac.jp

Keywords: *Chacana caldera, Oyacachi, Salve Faccha, geothermal exploration.*

ABSTRACT

Located at about 60 km east of Ecuador's capital, Chacana is an eroded Plio-Holocene resurgent caldera complex, considered one of the largest rhyolitic centers of the northern Andes. Between 2011 and 2012, two main geothermal prospects in the southern part of Chacana were identified. However, the northern part of the caldera remains unexplored, despite the existence of several geothermal manifestations in Salve Faccha and Oyacachi. Detailed geological mapping was conducted, focused on the identification of structural features, volcanic deposits, and hydrothermal features. Field observations were supplemented by XRD analysis, kinematic analysis, dilation potential estimation and literature review to refine the geochemical interpretation.

The volcanic deposits in the northern part of the Chacana Caldera record a prolonged period of activity during the Quaternary, with sequences of volcanic rocks overlying Paleozoic metamorphic basement. The Rosaspungo center, in particular, exhibits evolved magmatic activity, suggesting the presence of a shallow heat source capable of sustaining a convective geothermal system. Within the caldera, volcanoclastic deposits have developed secondary permeability due to a trans-pressional tectonic regime (ESE-trending σ_1), hosting a high-temperature (~230°C) geothermal reservoir controlled by NW-SE normal-sinistral faults. These structures, with the E-W faults, also facilitate fluid migration toward a secondary lower-temperature reservoir (~150°C) located beneath Oyacachi village, ~10 km to the east. Overlying the primary reservoir, the geothermal system develops a substantial cap rock characterized by Illite alteration which extends across ~2 km in diameter around the Salve Faccha lake. Approximately 17 hot springs were reported around and beneath the lake, discharging mostly Cl-Na type waters. In addition, HCO3-type hot springs and travertine deposits at Oyacachi village suggest the peripheral part of the system. These results confirm the existence of a convective geothermal system with favorable permeability and high enthalpy, positioning the Salve Faccha–Oyacachi prospect as a strategic resource for renewable energy generation for the capital city of Ecuador.

1. INTRODUCTION

Ecuador possesses abundant natural resources for energy production. Currently, hydroelectric power dominates the electricity generation, accounting for 63.45% of the total output in 2024 (ARCONEL, 2024). However, increasingly frequent and prolonged dry seasons in recent years have significantly reduced hydropower capacity, triggering recurrent energy crises and nationwide blackouts. In this context, geothermal energy emerges as a promising renewable alternative, with an estimated theoretical potential exceeding 2 000 MW (counting the number of active volcanoes according Stefansson (2005) methodology. Its development offers a reliable solution to diversify the national energy mix and accelerate the transition toward sustainable energy.

Ecuador hosts over 20 geothermal prospects distributed across six geothermal plays throughout the country (Figure 1A). Due to their geological characteristics, the most promising geothermal prospects for energy production are located in the Galápagos hotspot (GHS) and in the Northern Andes Highlands geothermal play (NAH) (Beate et al., 2020). The latter hosts more than 80 quaternary volcanoes (Bernard & Andrade, 2011) situated between the Cosanga (CCPP) and Quito-Latacunga fault systems (Figure 1B).

Chacana caldera is located ~60 km eastward from Quito (Figure 1B) in the NAH, is considered a Plio-Holocene rhyolitic resurgent caldera constructed on metamorphic basement from the eastern cordillera. It is composed by four main volcanic groups and is characterized by the Chacana Rift (Figure 1C), a prominent N–S suture structure that provided a major source of magma and eruptive activity during the Late Pleistocene (M. L. Hall & Mothes, 2008). Due to its geological characteristics, at least three geothermal prospects have been identified: Cachiyacu, Jamanco (southern part-high enthalpy), and Oyacachi (northern part-medium enthalpy) (Beate et al., 2011; MEER, 2010). Geoscientific investigations developed in the southern sector confirmed Cachiyacu and Jamanco as viable prospects for power generation (Beate & Urquizo, 2015); though with moderate development risk due to limited permeability (CELEC/SYR, 2012). Even though these investigations improve understanding of the caldera in its southern part; the northern portion is still poorly characterized without detailed geology and geochemistry.

In the following sections, we present compelling evidence that positions the Salve Faccha-Oyacachi geothermal system as one of the most promising prospects in the NAH, exhibiting favorable permeability characteristics and potential to host a high-enthalpy convective geothermal system.

2. METHODOLOGY

Geological mapping was developed in August 2024 and the lithostratigraphic framework was established following the classification defined by Hall & Mothes, (2008), supported on field observations and stratigraphic relationships. The sample collection focused on hydrothermal alteration zones and associated mineral deposits, which were analyzed using

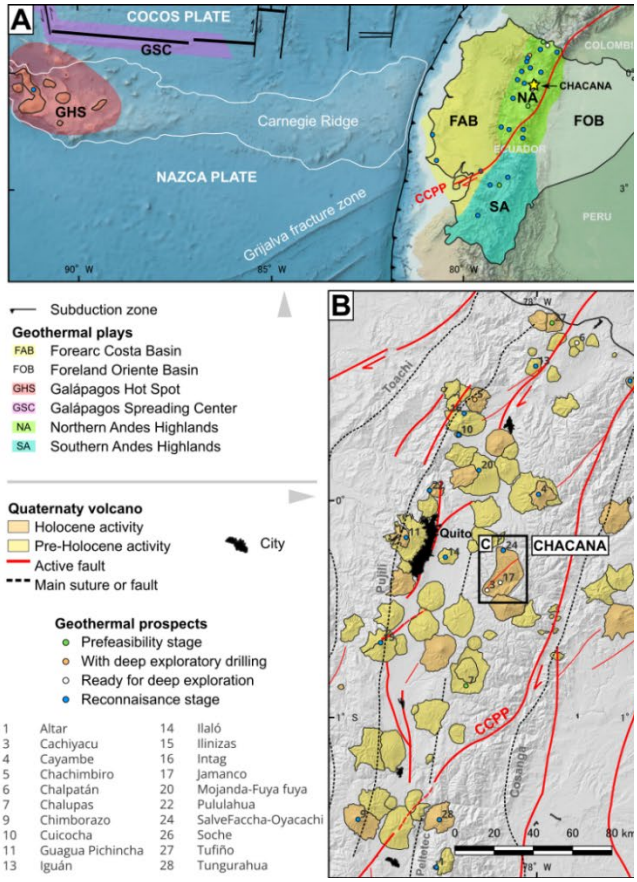

Figure 1. A. Location and status of geothermal prospects with the Geothermal Plays of Ecuador, from Beate et al., (2020). B. Distribution of the geothermal prospects along the NA geothermal play in contrast with the Ecuadorian volcanic arc (modified from Alvarado et al., 2016), and location of Chacana Geothermal Prospect. C. Geological and geochronological data of Chacana caldera compiled from Bigazzi et al. (2005); Hall & Mothes (2008); Opdyke et al. (2006); Santamaria et al. (2024) . Rigaku X-Ray Diffractometer. Sample preparation was conducted following Moore & Reynolds, (1990) and Poppe et al., (2001), using randomly oriented powders and oriented aggregates for accurate clay minerals identification.

Kinematic indicators were systematically characterized and classified following the criteria defined by Doblas, (1998); Mukherjee, (2015); Petit, (1987); and Tjia, (2014), considering the quality of shear sense indicators. The stress field inversion was performed using the Multiple Inversion Method software, developed by Yamaji et al., (2011). Dilation potential was assessed based on the orientation of faults relative to the minimum horizontal stress direction (SHmin), following the criteria of (Ferrill et al., 1999). For visualization purposes, the results were classified according to Shevenell et al., (2015).

Geochemical and isotopic data used in this study were compiled from (Carrera-Villacrés et al., 2016; Ibarra, 2025; INAMHI, 2013; Inguaggiato et al., 2010) Gorini, (2015); Parión, (2024). The characterization of geothermal fluids was performed using Schoeller diagrams and Cl–HCO_3–SO_4 plots to identify water types and potential mixing processes. The Na–K–Mg ternary diagram was employed to evaluate the chemical equilibrium of the fluids with the reservoir, as well as to estimate the resource temperature. Fluid origins and recharge zones were inferred from δ^2H–$\delta^{18}O$ data and elevation. Diagrams were generated using Python.

3. RESULTS AND DISCUSSION

3.1 Geology

The northern part of the Chacana caldera was constructed over NNE foliated Paleozoic metamorphic basement and strongly fractured Miocene volcanic products from the Pisayambo Formation. It outcrops eastward of Oyacachi town, Figure 2. The metamorphic rocks are medium-grained schists [Qz+Ser] and gneisses [Qz+Ser+Chl+Grt], associated with the Agoyan unit (Litherland et al., 1994). On the other hand, Pisayambo Formation is composed by porphyritic andesites.

In the northern part of Chacana Caldera, Group 1 crops out near Oyacachi town, downstream at the Turnofaccha waterfall, Figure 2. It exposes pyroxene-bearing andesitic lava flows, locally displaying a vuggy texture that is occasionally filled with calcite. In the southwestern portion of the study area the oldest rocks of Chacana were dated 40Ar/39Ar between 2.15 ± 0.19 and 2.71 ± 0.19 Ma (Opdyke et al., 2006). Group 2 consists of over 500 m of outer flank deposits, primarily exposed along the road to Oyacachi, Figure 2. These include matrix-supported Ignimbrite deposits and spherulites which are overlayed by porphyritic andesite lava flows (locally obsidian flows). Lava flows which overlay ignimbrite deposits were dated between 1.77 ± 0.24 – 0.81 ± 0.05 Ma (Bigazzi et al., 2005; Opdyke et al., 2006) in the western flank of Chacana (Figure 1C).

Group 3 comprises the caldera infilling volcanic units and has been subdivided into four subunits based on field and petrographic characteristics, Figure 2. Unit 3A -Mogotes unit, with the best exposures around Mogotes lake, below 4100 masl, and is at least 300 m thick. It consists of altered matrix-supported polylithic volcanic breccia with centimetric angular intermediate volcanic clasts, including juvenile tuffs. Petrographic analysis revealed propylitic alteration [Chl+Cal+Zeo+Py+Cpy] with palagonitization, often associated with phreatomagmatic activity (McPhie et al., 1995; Stroncik & Schmincke, 2002). The overlying Unit 3B is composed of vitrophyres and porphyritic andesite lava flows with two pyroxenes, exhibiting localized alteration [Zeo+Cal]. Unit 3C is exposed to below 3680 masl, with an estimated thickness of ~200 m. Well exposures are in the Salve faccha waterfall. It consists of well-compacted, matrix supported andesitic breccia. The composition of the clasts closely matches the lava flows of Unit 3B, suggesting a shared magmatic origin; however, further geochemical studies may clarify the source of this deposit. Fluvial deposits of Unit 3D unconformably overlies the sequence and shows lateral thickness variation from 6 to ~20 m, also observable at Salve Faccha waterfall. It is composed at the base for conglomerates overlayed by interbedded tuffaceous siltstones and sandstone. Phreatomagmatic maar deposits identified in the upper part of Unit 3A (Enríquez & Morales, 2017) have been dated in the southwestern portion of the study area, showing a range of ages (Opdyke et al., 2006); however, the most consistent with the caldera's evolution is 0.45 ± 0.08 Ma.

Group 4 preserves the last volcanic activity shown in the northern part of Chacana caldera and was subdivided into three units. Units 4A and 4B correspond to the construction of silicic volcanic centers, Mullumica and Callejones. Unit 4A consist of porphyritic andesite lava flows, vitrophyres with localized obsidian flows and discrete pyroclastic flows, while voluminous obsidian flows characterize unit 4B. Fission track dating indicates 0.22 ± 0.02 Ma and 0.17 ± 0.01 – 0.20 ± 0.02 Ma (Bigazzi et al., 2005) for Units 4A and 4B, respectively. Unit 4C shows the last effusive period in the northern part of Chacana, comprising basaltic andesite lava flows that extend for over 9 km outside and within the caldera. Geochronological data reveal 39 ka and 21 ka (M. Hall et al., 2000, green and orange, respectively, in Figure 1C).

3.2 Structural Geology & Dilation Potential

Structural data collected across all lithostratigraphic units of the Chacana Caldera reveal distinct fault patterns, as illustrated in Figure 3 and summarized in Table 1. The stratigraphic differentiation enables the identification of E–W-trending faults as concealed structures, since they are only exposed within Group 3 deposits and are buried beneath the Group 4. On the other hand, the eruptive centers on the western flank of the caldera coincide with the intersection of NE–SW and E–W faults (Figure 2). These centers align along the interpreted Chacana Rift (Figure 1C).

Stress inversion results showed a transpressional tectonic regime [σ1: 107.6/28.7; σ3: 219.2/33.9; φ: 0.3], consistent with previous regional models proposed for the northern Ecuadorian Andes (e.g. Ego et al., 1996). According to Ferrill et al. (1999), faults oriented at high angles to the minimum horizontal stress direction (SHmin) are more favorable for dilation and enhanced permeability.

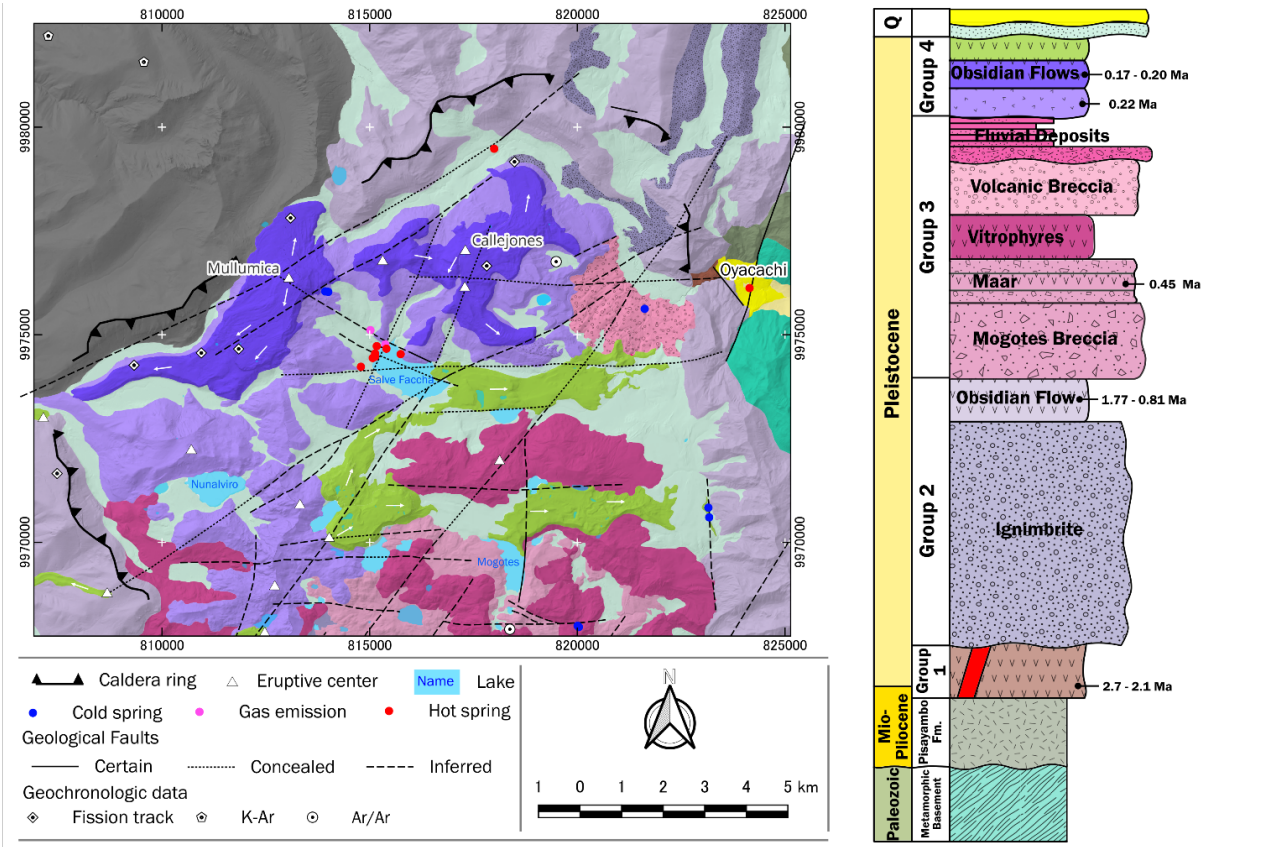

Figure 2: Left: Geological Map of the study area in the northern part of Chacana Caldera, with the main geothermal manifestations. Right: Lithostratigraphic column (not at scale). For geochronological data see Figure 1.

In this context, the NW–SE and E–W fault sets are interpreted as the most permeable (Figure 3). This interpretation is consistent with field observations, where hot springs in the Salve Faccha are aligned in the same direction.

Unit	Code	Faults Type	Direction/Dip
Basement	A	Dextral	NNE/SE
2 – Outer flank deposits	B	Normal	NW-SE/NE
	C	Dextral	NE-SW/NW
3 – Infilling material	E	Reverse – strike slip	N-S/E
	F	Dextral-Normal	E-W/N
4 – Lava emission	D	Normal-Sinistral	NW-SE/SW

Table 1: Summary of geological faults identified.

3.3 Hydrothermal alteration and associated deposits

Hydrothermal alteration is clearly observed in the unit 4A around the Salve Faccha and Mogotes lakes, spatially associated with E–W and NW–SE-trending faults. XRD analyses (Figure 4; Table 2) reveal distinct mineralogical

assemblages across the Salve Faccha area. In the eastern sector of the lake, illite, kaolinite, and smectite-dominated mixed-layer clays were identified, suggesting the presence of an upper argillic alteration zone (<180 °C) typically associated with caprock conditions with least permeability (Stimac et al., 2015). In contrast, the western side is characterized by illite and chlorite, indicative of a transition zone (>180 °C) with low permeability (Stimac et al., 2015).

The Mogotes area is characterized by illite–smectite (I/S) mixed-layer clays and chlorite. The association of zeolites and calcite in unit 3A, extending into unit 3B, alongside I/S clays, indicates low to moderate hydrothermal temperatures consistent with a transitional alteration zone (Stimac et al., 2015). In contrast, hydrothermal deposits near Oyacachi town, closely linked to nearby hot springs, and farther east along the upper Quebrada Derrumbo consist of travertine calcite rich, Figure 4. Their exposures are limited by landslides which cover the deposits. Additionally, smectite and kaolinite were detected near a geological fault, suggesting low-temperature alteration; the presence of kaolinite likely reflects supergene weathering processes enhanced by structural permeability in the fault zone.

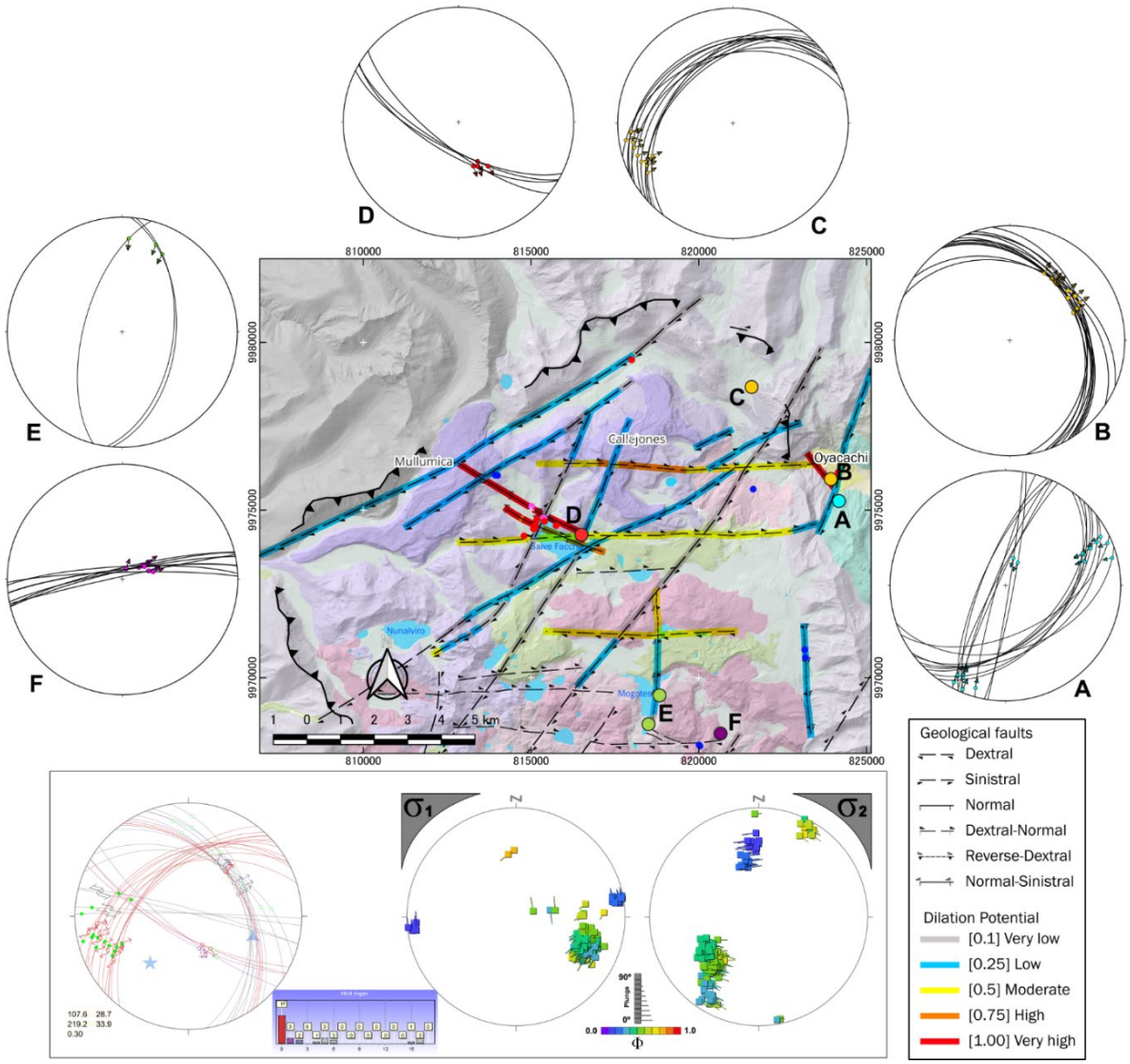

Figure 3. Geological faults detected in the study area and Dilation Potential map for the Salve Faccha and Oyacachi areas calculated through the results of the stress inversion using the Multiple Inverse Method (bottom).

Unit	Sample	Treatment	Main Peaks (d-spacing Å)	Interpretation	Supporting Features	Reference
4A	XA26 M1	Untreated	15.0, 10.0, 7.15, 3.58, 3.54	Smectite in I/S, minor illite and Kaolinite	Broad ~15 Å peak, slight 10 Å contraction. Doublet 3.58 & 3.54 Å	[1], [2]
		Glycolated	15.0, 9.8, 7.15, 3.58, 3.54			
	XA26 M2	Untreated	10.7, 5.27, 3.3, 3.2	Illite	Peaks remain unaltered	[4]
		Glycolated	10.9, 5.2, 3.34, 3.2			
	XA28 M2	Untreated	9.9, 7.24, 3.59	Illite + Chlorite	Peaks remain unaltered No doublet peaks.	[1], [2], [3], [4]
		Glycolated	10, 7.27, 3.6			

3A	XA18 M1	Untreated	10.8, 7.1, 3.58	Illite-smectite mixed-layer (I/S)	10.8 Å → 9.7 Å (contraction); 7.1 Å stable	[1], [2]
		Glycolated	9.7, 7.1, 3.58			
	XA14 M1	Untreated	14.7, 7.24, 3.58	Chlorite	Peaks remain unaltered	[1], [3]
		Glycolated	14.72, 7.22, 3.57			
2	XA03 M2	Untreated	14.53, 7.24, 3.59	Smectite and Kaolinite	Expansion from 14 Å → 17Å typical smectite. Kaolinite stable	[1], [2], [3], [4]
		Glycolated	17.87, 7.23, 3.59			

Table 2. Interpretation of XRD clay-oriented samples. Salve Faccha (XA26M1, XA26M2, XA28M2), Mogotes (XA14M1, XA18M1) and Oyacachi (XA03M2). [1](Brindley, 1955; Moore & Reynolds, 1990; Poppe et al., 2001; Srodon, 1980).

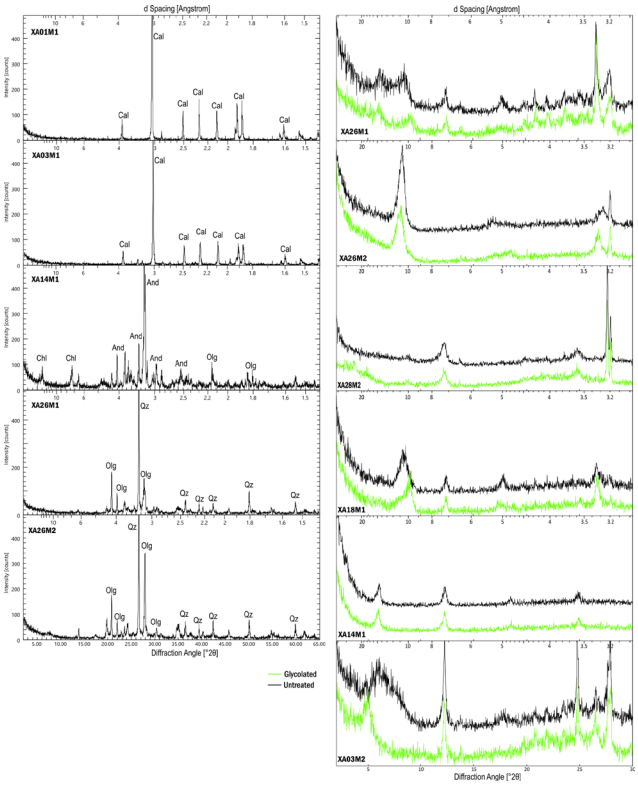

Figure 4. XRD results of Salve Faccha (XA26M1, XA26M2, XA28M2), Mogotes (XA14M1, XA18M1) and Oyacachi (XA01M1, XA03M1, XA03M2). Left: bulk analysis; right: clay-oriented analysis.

3.4 Contributions for the volcano-tectonic evolution

We support that NNE dextral faults were also responsible for the caldera formation, followed by an explosive event that deposited the outer flank deposits at around 1Ma. Then the continuous interaction between groundwater and magma produced the phreatomagmatic Mogotes unit; at this time the volcanic activity did not stop which is represented by the multiple lava flows who cover the Mogotes unit. Altogether and considering the fluvial deposits which uncomformably overly the previous units, support that a resurgence stage happened in the caldera. At this time E-W and N-S faults were developed as ring faults due to the rise of the caldera floor. At the end of Pleistocene, the volcanic activity continued, and two main silicic volcanic centers were constructed, Mullumica and Callejones. The final basaltic lava emission runs for several kilometers outside and within the caldera covering the previous deposits. Finally, the tectonic setting was established with the NE-SW faults and the volcanic deposits within the caldera were shaped during the pleni and tardi-glaciar within the northern part of the Chacana caldera.

3.5 Geochemistry

The Salve Faccha area hosts more than a dozen bubbling hot springs, reaching temperatures of up to 66 °C with neutral pH, along with two zones of H_2S gas emissions, one of which is associated with a cold spring and lightly acidic conditions. These geothermal manifestations are predominantly aligned in a NW trend, consistent with faults mapped in the surrounding area with the same direction (Figure 3). On the other hand, Oyacachi contains bubbling hot springs with temperatures up to 46 °C and neutral pH.

The Schoeller diagram (Figure 5A) shows that most Salve Faccha samples (yellow lines) are dominated by Cl^-–Na^+, whereas Oyacachi samples (black lines) display HCO_3^-–Na^+ composition. Both groups have similar total dissolved solids and parallel trends, but they differ markedly in Ca and Mg contents. In Salve Faccha, Ca concentrations are generally <20 mg/L, while in Oyacachi they reach up to 219 mg/L (Ibarra, 2025). Compared with reference values for geothermal reservoir fluids (<50 mg/kg; Nicholson (1993); here mg/L and mg/kg are treated as equivalent by assuming a density close to 1 g/cm³), the low Ca contents in Salve Faccha are consistent with high-temperature fluid conditions, whereas the higher values in Oyacachi indicate stronger interaction with shallow bicarbonate waters. Likewise, Mg concentrations in Salve Faccha are mostly <0.1 mg/L, compared to 65–77 mg/L in Oyacachi (Ibarra, 2025). The low Mg values in Salve Faccha fall within the range expected for high-temperature geothermal fluids (0.01–0.1 mg/kg; Nicholson, 1993), while the elevated Mg in Oyacachi again suggests greater mixing with shallow groundwater during lateral flow. The Cl–HCO_3–SO_4 ternary diagram (Figure 5B) supports this interpretation, placing Salve Faccha samples close to the mature Cl–Na water zone, which appears with higher temperatures than those of Oyacachi samples, which fall within the diluted Cl–HCO_3 field.

Na–K–Mg diagram (Figure 5C) shows that the waters from Salve Faccha are in a state of partial equilibrium, close to full equilibrium, with an average temperature of 230 °C. In contrast, the Oyacachi samples plot within the immature water field, indicating a lower degree of geochemical equilibrium and significantly lower temperatures compared to those from Salve Faccha. Therefore, samples from Salvefaccha are closer to the upflow zone. This interpretation is supported also by the Na/K ratio of approximately 10 (Ibarra, 2025), which is associated with high-temperature and upflow zones (Nicholson, 1993),. Conversely, the samples from Oyacachi display the common features of an outflow zone. The waters are HCO_3-type, reflecting mixing with shallow groundwater and partial neutralization of rising CO_2-rich fluids (Giggenbach, 1991). Geothermometric estimates show lower reservoir temperatures, consistent with conductive cooling and dilution during ascent (Fournier,

1977). The occurrence of travertine deposits supports this interpretation.

The isotopic composition (Figure 5D) shows $\delta^{18}O$ values between −12 and −10‰ and δD values between −89 and −75‰, clustering closely along the Global Meteoric Water Line. This pattern indicates a meteoric origin. In contrast, few samples of Oyacachi and Salve Faccha have shown isotopic shift of oxygen, suggesting the occurrence of enhanced water–rock interactions (Inguaggiato et al., 2010). On the other hand, δD becomes progressively more negative with elevation. Sample values (≈ −89 to −85‰) correspond to recharge elevations of approximately 4100 masl. Based on the findings presented, water samples from Salve Faccha and Oyacachi appear to share the same hydrothermal origin.

4. CONCLUSION

Figure 6 shows the preliminary geothermal conceptual model of Salve Faccha – Oyacachi prospect. Continuous silicic volcanic activity during the late Pleistocene (Mullumica and Callejones), contributed to the formation of shallow heat source around Salve Faccha lake.

Recharge of the geothermal system is estimated to occur at elevations of ~4100 masl, where meteoric waters infiltrate through deep geological faults, particularly those striking NE. The upflow zone is inferred to be located at the western margin of the Salve Faccha lake, where fluids ascend through NW–SE and E–W most permeable fault systems. These structures cut volcaniclastic deposits and lava flows of Groups 1 and 3 of the Chacana Caldera; in addition, they intersect with other faults creating a complex tectonic setting with favorable fractured reservoir. Continuous water–rock interaction within this reservoir has formed a convective hydrothermal system characterized by Na–Cl waters equilibrated at ~230 °C, enclosed by an Illite-rich clay cap. From the reservoir, geothermal fluids migrate laterally eastward along E–W faults, where volcanic units of Group 4 act as a secondary cap rock that blocks them from reaching the surface. Finally, the fluids discharge through NW–SE normal faults near Oyacachi town, where HCO_3-type hot springs and associated travertine deposits clearly mark the outflow zone of the system.

Considering the extent of the clay cap, a preliminary potential estimate can be made based on the inferred reservoir area (Wilmarth & Stimac, 2015). Using a conservative estimation of ~2 km² beneath the Salve Faccha sector, and accounting the geological controls of the system, the reservoir could host a minimum capacity of ~20 MW and a maximum potential of up to ~60 MW.

ACKNOWLEDGEMENTS

We extend our sincere gratitude to our colleagues at Kyushu University and the Ecuadorian Geothermal Association for their insightful discussions and valuable contributions throughout the development of this study. Special thanks are due to the Japan International Cooperation Agency (JICA) for supporting this research through the KIZUNA Program. We are also deeply grateful to the community of Oyacachi for their collaboration, hospitality, and genuine interest in the future use of geothermal energy. Last but not least, we thank our families for their unwavering support and encouragement.

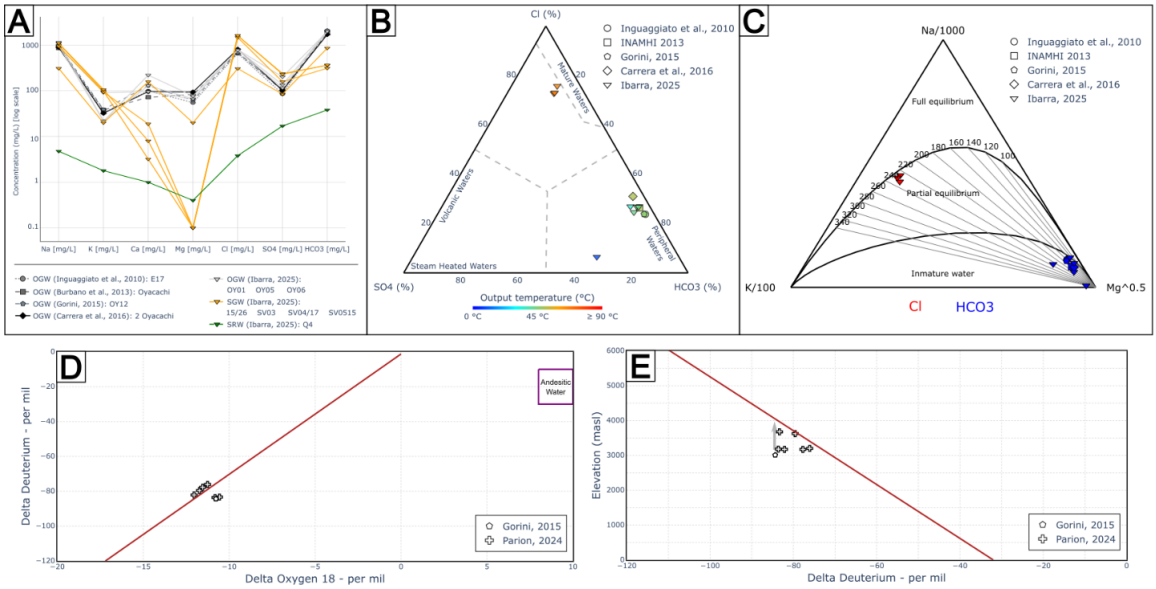

Figure 5. A. Schoeller diagram showing Oyacachi Geothermal Water: OGW, Salve Faccha Geothermal Water: SGW and Salve Faccha River Water: SRW. B Cl–HCO_3–SO_4 ternary diagram. C. Na–K–Mg diagram. D. δD vs $\delta^{18}O$ diagram. E. Elevation vs δD in hot springs for Salve Faccha and Oyacachi area.

ISSN 2703-4275

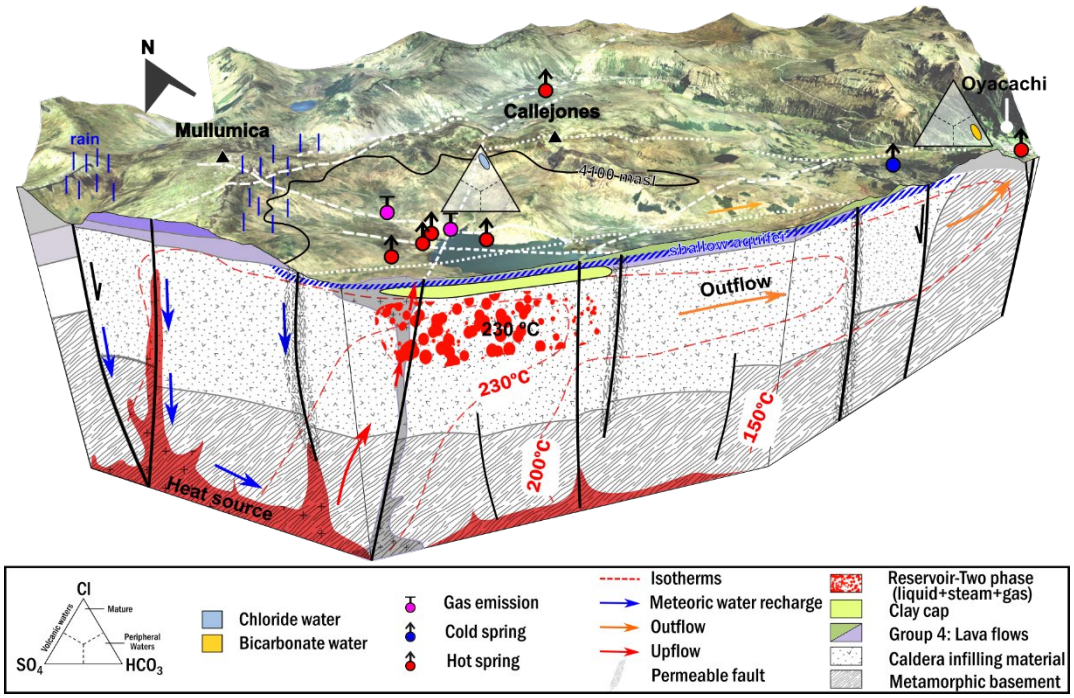

Figure 6. Preliminary Geothermal Conceptual Model of the Salve Faccha-Oyacachi geothermal prospect.

REFERENCES

Alvarado, A., Audin, L., Nocquet, J. M., Jaillard, E., Mothes, P., Jarrín, P., Segovia, M., Rolandone, F., & Cisneros, D. (2016). Partitioning of oblique convergence in the Northern Andes subduction zone: Migration history and the present-day boundary of the North Andean Sliver in Ecuador. *Tectonics*, *35*(5), 1048–1065. https://doi.org/10.1002/2016TC004117

ARCONEL. (2024). Estadística Anual y Multianual del Sector Eléctrico Ecuatoriano. *Documento Preliminar*.

Beate, B., & Urquizo, M. (2015). Geothermal country update for Ecuador, 2010–2015. *Proceedings World Geothermal Congress Melbourne, Australia.*, *April*, 19–25.

Beate, B., Urquizo, M., & Lloret, A. (2020). Geothermal Country Update of Ecuador: 2015-2020. *Proceedings World Geotermal Congress 2020, Reykjavic, Iceland*, *1*, 1–13.

Beate, B., Villares, F., Inguaggiato, S., Hidalgo, S., & Benitez, S. (2011). *Modelo geotérmico preliminar de tres áreas de interés en la caldera cuaternaria resurgente de chacana y estimación teórica de su potencial geotermoeléctrico*. *1*, 70–91. http://bibdigital.epn.edu.ec/handle/15000/5628

Bernard, B., & Andrade, D. (2011). Volcanes Cuaternarios del Ecuador Continental. *IGEPN Poster Informativo*.

Bigazzi, G., Hadler Neto, J. C., Iunes, P. J., & Osório Araya, A. M. (2005). Fission-track dating of South American natural glasses: An overview. *Radiation Measurements*, *39*(6), 585–594. https://doi.org/10.1016/j.radmeas.2004.09.006

Brindley, G. W. (1955). Identification of Clay Minerals by X-Ray Diffraction Analysis. *Clays and Clay Technology (National Conference on Clays and Clay Technology)*, *1*, 119–129. https://doi.org/10.1346/ccmn.1952.0010116

Carrera-Villacrés, D., Hidalgo, A., Guevara-García, P., Vivero, M. T., & Delgado-Rodríguez, V. (2016). Hydrogeochemical analysis of volcanic and geothermal fluids in the Andes from Ecuador using hydrochemical plots (Stiff, Piper and Schoeller-Berkaloff diagrams). *IOP Conference Series: Earth and Environmental Science*, *39*(1). https://doi.org/10.1088/1755-1315/39/1/012062

CELEC/SYR. (2012). Estudio de Prefactibilidad Inicial para Elaborar el Modelo Geotérmico Conceptual del Proyecto Chacana. *Informe Técnico No Publicado Preparado Por SYR*, 183.

Doblas, M. (1998). Slickenside kinematic indicators. *Tectonophysics*, *295*(1–2), 187–197. https://doi.org/10.1016/S0040-1951(98)00120-6

Ego, F., Sébrier, M., Lavenu, A., Yepes, H., & Egues, A. (1996). Quaternary state of stress in the Northern Andes and the restraining bend model for the Ecuadorian Andes. *Tectonophysics*, *259*, 101–116. https://doi.org/10.1016/0040-1951(95)00075-5

Enríquez, Y., & Morales, K. (2017). *Estudio Litoestratigráfico y de alteraciones hidrotermales en los testigos de perforación de los pozos TTC-2, TTC-3 y TTC-9, del interior de la Caldera de Chacana, Provincias de Napo y Pichincha* [Tesis, Escuela Politécnica Nacional]. http://bibdigital.epn.edu.ec/bitstream/15000/14623/1/CD-6793.pdf

Ferrill, D. A., Winterle, J., Wittmeyer, G., Sims, D., Colton, S., Armstrong, A., Horowitz, A. S., Meyers, W. B., & Simons, F. F. (1999). Stressed Rock Strain

Groundwater at Yucca Mountain, Nevada. *GSA Today*, *9*(5), 2–9.

Fournier, R. O. (1977). Chemical geothermometers and mixing models for geothermal systems. *Geothermics*. https://doi.org/10.1016/0375-6505(77)90007-4

Giggenbach, W. (1991). Chemical techniques in geothermal exploration. *Application of Geochemistry in Geothermal Reservoir Development*, 119–144. https://cir.nii.ac.jp/crid/1570572699730688640.bib?lang=en

Gorini, A. (2015). Heat source and reservoir of geothermal areas in Latin America as inferred from thermobarometry of amphibole bearing extrusives and fluid geochemistry: examples from Chile and Ecuador. *PhD. Thesis. Universita Degli Studi Di Urbano Carlo Bo*, 106.

Hall, M. L., & Mothes, P. A. (2008). The Chacana caldera complex in Ecuador. In *IOP Conference Series: Earth and Environmental Science* (Vol. 3, p. 012004). https://doi.org/10.1088/1755-1307/3/1/012004

Hall, M., Mothes, P., & J., C. (2000). El Complejo Caldérico de Chacana – Ecuador. *Poster*.

Ibarra, D. (2025). Assessment of Geothermal Energy and Lithium Co-Production Potential in Salvefaccha-Oyacachi, El Hondón, and Salinas de Bolívar, Ecuador. *Master Thesis, Department of Cooperative Program for Resources Engineering. Kyushu University, Japan.*, *February*.

INAMHI. (2013). Aguas termominerales en el Ecuador. *Estudio Realizado Por Burbano M., Becerra S. Pasquel E.*, 96.

Inguaggiato, S., Hidalgo, S., Beate, B., & Bourquin, J. (2010). Geochemical and isotopic characterization of volcanic and geothermal fluids discharged from the Ecuadorian volcanic arc. *Geofluids*, *10*(4), 525–541. https://doi.org/10.1111/j.1468-8123.2010.00315.x

Litherland, M., Aspden, J. A., & Jemielita, R. A. (1994). The Metamorphic Belts of Ecuador. *British Geological Survey*.

McPhie, J., Doyle, M., & Allen, R. (1995). Volcanic textures: A guide to the interpretation of textures in volcanic rocks. *Journal of Volcanology and Geothermal Research*, *64*(3–4), 328–329. https://doi.org/10.1016/0377-0273(95)90002-0

MEER. (2010). Plan para el aprovechamiento de los recursos geotérmicos en el Ecuador. *Unp.Tech.Report Prepared by B.Beate.*, *589 2*.

Moore, D. M., & Reynolds, R. C. (1990). X-ray Diffraction and the Identification and Analysis of Clay Minerals. *Clays and Clay Minerals. Oxford University Press*, *38*(4). https://doi.org/10.1346/ccmn.1990.0380416

Mukherjee, S. (2015). Brittle Faults. In *Atlas of Structural Geology* (pp. 79–106). https://doi.org/10.1016/b978-0-12-420152-1.00003-x

Nicholson, K. (1993). Geothermal Fluids. Chemistry and Exploration Techniques. *Xv + 263 Pp. Berlin, Heidelberg, New York, London, Paris, Tokyo, Hong Kong: Springer-Verlag.* https://doi.org/10.1017/s0016756800011535

Opdyke, N. D., Hall, M., Mejia, V., Huang, K., & Foster, D. A. (2006). Time-averaged field at the equator: Results from Ecuador. *Geochemistry, Geophysics, Geosystems*, *7*(11). https://doi.org/10.1029/2005GC001221

Parión, C. (2024). Estudio Geológico del Reservorio Geotérmico de Oyacachi, Provincia de Napo, Ecuador. *UCE Thesis*, 147.

Petit, J. P. (1987). Criteria for the sense of movement on fault surfaces in brittle rocks. *Journal of Structural Geology*, *9*(5–6), 597–608. https://doi.org/10.1016/0191-8141(87)90145-3

Poppe, L. J., Paskevich, V. F., Hathaway, J. C., & Blackwood, D. S. (2001). A Laboratory Manual For X-Ray Powder Diffraction. *US Geological Survey Open-File Report 1.041*, 1–88.

Santamaria, S., Bablon, M., Quidelleur, X., Samaniego, P., Le Pennec, J. L., Hidalgo, S., & Liorzou, C. (2024). Blossoming of the Pleistocene volcanism in the Ecuadorian Andes: a review based on new and recent geochronological data. *Bulletin of Volcanology*, *86*(9), 1–62. https://doi.org/10.1007/s00445-024-01767-z

Shevenell, L., Coolbaugh, M., Hinz, N., Stelling, P., Melosh, G., & Cumming, W. (2015). *Geothermal Potential of the Cascade and Aleutian Arcs, with Ranking of Individual Volcanic Centers for their Potential to Host Electricity- Grade Reservoirs*. 152.

Srodon, J. (1980). Precise identification of illite/ smectite interstratifications by X-ray powder diffraction. *Clays & Clay Minerals*. https://doi.org/10.1346/CCMN.1980.0280601

Stefansson, V. (2005). World Geothermal Assessment. *Proceedings World Geothermal Congress Anatalya, Turkey.*, *April*, 24–29.

Stimac, J., Goff, F., & Goff, C. J. (2015). Intrusion-Related Geothermal Systems. In *The Encyclopedia of Volcanoes* (pp. 799–822). Elsevier. https://doi.org/10.1016/B978-0-12-385938-9.00046-8

Stroncik, N. A., & Schmincke, H. U. (2002). Palagonite - A review. *International Journal of Earth Sciences*, *91*(4), 680–697. https://doi.org/10.1007/s00531-001-0238-7

Tjia, H. D. (2014). Fault-plane markings as displacement sense indicators. *Indonesian Journal on Geoscience*, *1*(3), 151–163. https://doi.org/10.17014/ijog.v1i3.177

Wilmarth, M., & Stimac, J. (2015). Power Density in Geothermal Fields. *Proceedings World Geothermal Congress 2015*, *April*, 1–7.

Yamaji, A., Sato, K., & Otsubo, M. (2011). Multiple Inverse Method Software Package. *Division of Earth & Planetary Sciences, Kyoto University*, 1–16.

ISSN 2703-4275